PAN
ARCHIVES OF ACOUSTICS
Vol. **44**, No. 4, pp. 625–636 (2019)
DOI: 10.24425/aoa.2019.129721

Research Papers

The Effect of Dynamic Beam Deflection and Focus Shift on the Acoustic Field Distribution Inside the Ultrasonic Ring Array

Wiktor STASZEWSKI*, Tadeusz GUDRA, Krzysztof J. OPIELIŃSKI

Department of Acoustics and Multimedia
Faculty of Electronics
Wrocław University of Science and Technology
Wybrzeże Wyspiańskiego 27, 50-370 Wrocław, Poland
e-mail: {tadeusz.gudra, krzysztof.opielinski}@pwr.edu.pl
*Corresponding Author e-mail: wiktor.staszewski@pwr.edu.pl

(*received May 26, 2019; accepted August 24, 2019*)

This paper presents the results of acoustic field distribution simulations for the 1024-element ultrasonic ring array intended for the diagnosis of female breast tissue with the use of ultrasound tomography. For the purpose of analysing data, all acoustic fields created by each elementary transducer were combined. The natural position of the focus inside the ultrasonic ring array was changed by altering activation time of individual transducers in sectors consisting of 32, 64, and 128 ultrasonic transducers. Manipulating the position of the focus inside the array will allow to concentrate the ultrasonic beam in a chosen location in the interior space of the ring array. The goal of this research is to receive the best possible quality of images of cross-sections of the female breast. The study also analysed the influence of the acoustic field distribution on the inclination of the beam. The results will enable to choose an optimal focus and an optimal number of activated transducers.

Keywords: ultrasonic ring array; acoustic field distribution; ultrasonic beam focusing; ultrasound tomography.

1. Introduction

Ultrasound tomography enables early detection of pathologies in biological tissues and recognition of malignant neoplasia. There are currently several research centres around the world that develop prototypes of ultrasound tomography scanners (Birk *et al.*, 2016; Duric *et al.*, 2007a; 2013; Gudra, Opieliński, 2006a; 2006b; 2006c; Jirik *et al.*, 2012; Marmarelis *et al.*, 2007; Opieliński *et al.*, 2015; 2016; Wiskin *et al.*, 2013). Scientists from Wrocław University of Science and Technology (Gudra, Opieliński, 2006a; 2006b; 2006c; Opieliński *et al.*, 2014; 2015; 2016; 2018; Staszewski *et al.*, 2018) in coordination with the company Darmiński S.A. are conducting research into using ultrasound tomography for female breast diagnosis. Analysis of the acoustic field generated by elementary transducers of the ring array is significant in order for the ultrasound scanner to acquire the best possible image of the cross-section of the breast (by proper beam forming). The goal of this research is to analyse the acoustic field distribution during dynamic focusing of the ultrasonic beam. By changing the time of the activation of ultrasonic transducers, the location of the focus inside the ultrasonic ring array was also changed. During research, an attempt was made to use the ring array, adapted for use in ultrasound transmission tomography, whose individual transducers operate at a frequency of 2 MHz for ultrasound B-mode reflection imaging. The results will be applied in the full angle ultrasound spatial compound imaging (FASCI) method (Opieliński *et al.*, 2014). In an earlier publication on the same ultrasonic ring array, a full analysis was conducted of the acoustic field during natural focusing resulting from the curvature of the transducer template. The analysis of earlier results on the acoustic field distribution inside the ultrasonic ring array (Staszewski *et al.*, 2018) demonstrated that the optimal number of transducers in a sector, enabling to obtain ultrasound images using linear B-mode scanning, is $32 \leq n \leq 128$, thanks to the compromise between quality and the time of image acquisition. This paper analyses the inclination and focusing of ultrasonic beam generated

by 32, 64, and 128 transducers and analyses the ultrasound B-mode images acquired during the measurements of the wire pattern with one activated ultrasonic ring array section (subarray) comprised of 32 elementary ultrasonic transducers.

2. Construction of the ultrasonic ring array

The ring array used in ultrasonic tomography is composed of 1024 elementary piezoceramic transducers that operate at a frequency of approx. 2 MHz (Gudra, Opieliński, 2006a; 2006b; 2006c; Opieliński *et al.*, 2015; 2018). The transducers are in the shape of rectangular pillars measuring 0.5×18 mm and are approx. 1 mm thick. They are evenly distributed with the pitch of 0.3 mm on the inner side of the ring with the radius of $R_p = 130$ mm. Each elementary transducer can function as both a transmitter and a receiver. An example of a wire pattern submerged in water inside the array ring is presented in Fig. 1.

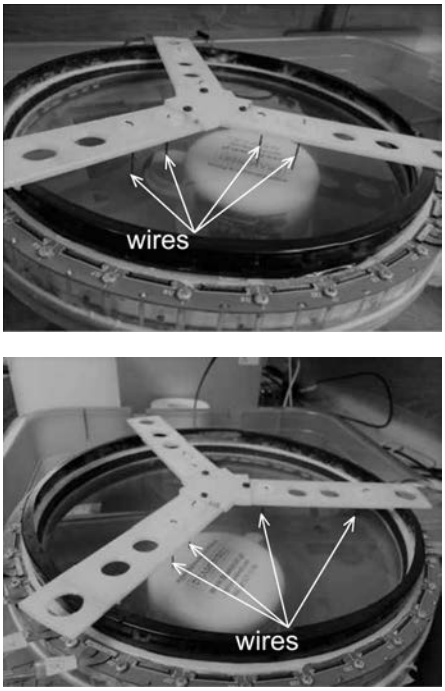

Fig. 1. Ultrasonic ring array together with the wire pattern submerged in water that were used in calculations, as viewed from top.

3. Calculation method

The ultrasonic ring array can work in water. For the purpose of measuring the acoustic field distributions created by the elementary ultrasonic transducers, the probe was submerged in distilled water with the temperature of 25°C. Water acts as a medium matching the elementary transducers of the array and the biological medium, that is breast tissue diagnosed *in vivo*.

For the sector of the multi-element array (subarray), in which the elementary transducers are distributed on the inner side of the ring, an algorithm was developed using MATLAB software to determine the distribution of pressure of an ultrasonic wave on any surface of the medium in the far field, generated by the concave curvilinear structure of rectangular ultrasonic transducers as a sum of geometric transformations of fields calculated for all the elementary transducers of the sector (Fig. 2).

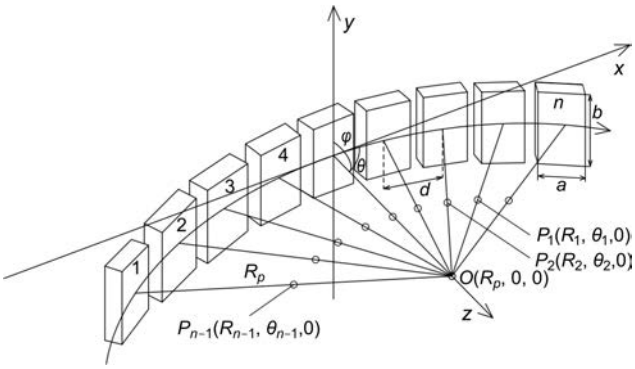

Fig. 2. Geometry of the ultrasonic ring array sector showing the sum of acoustic fields of the sector transducers.

For this purpose, the following equation was applied (Opieliński, 2011):

$$L_p = 20 \cdot \log \left[\left| \sum_{i=0}^{n-1} -\frac{j\rho ckV_a}{2\pi R_i} ab \cdot e^{j(\omega t - kR_i)} \left(\frac{\sin\left(\frac{u_i a}{2}\right)}{\frac{u_i a}{2}} \right) \cdot \left(\frac{\sin\left(\frac{wb}{2}\right)}{\frac{wb}{2}} \right) \right| \cdot \frac{1}{p_o} \right], \tag{1}$$

where L_p is the sound pressure level at point $P(R, \theta, \varphi)$, ρ is the density of the medium, c is the ultrasonic wave propagation velocity in the medium, $k = 2\pi/\lambda$ is the wave number, $\lambda = c/f$ is the wavelength, f is the resonance frequency of the ring array transducers, $\omega = 2\pi f$ is the cycle resonance frequency of pulsations, t is the time, V_a is the acoustic velocity, p_o is the reference pressure ($p_o = 1$ μPa), a is the width of the elementary rectangular transducer, b is the length of the elementary rectangular transducer, n is the number of transducers in the ring array sector (subarray), $u_i = 2\pi \cdot \sin(\theta_i)/\lambda$, $w = 2\pi \cdot \sin(\varphi)/\lambda$, R_i, θ_i, φ are polar coordinates of the point $P(R, \theta, \varphi)$, corrected in respect of the location $(i+1)$-th transducer in sector.

The far field in the horizontal plane of the rectangular elementary transducer with the width of $a = 0.5$ mm for a resonance frequency of $f_r = 2$ MHz is $l_o = 0.35a^2/\lambda \approx 0.12$ mm. Formula (1) enables precise calculations of the acoustic pressure level outside of the near field. The range of the near field is 0.12 mm, hence a precise analysis of the acoustic field along the central transducer axis in a horizontal plane is possible further away than this distance.

The geometrical transformation of the location of every point of the field $P(R,\theta,\varphi)$ in Eq. (1) is carried out symmetrically for every $(i+1)$-th transducer in the ring array sector (Fig. 2) by turning the point around the symmetry axis of the probe with coordinates $O(r = R_p,\ \theta = 0)$ parallel to the Y axis (where R_p denotes the probe's internal radius) by an appropriate multiplicity of the angle $\beta = i\cdot 2\pi/N$ (where N is the number of all the transducers in the ring array). Corrected this way, the complex values of the pressure are then summed for all the n sub-array elements, giving us the resultant pressure in each point $P(R,\theta,\varphi)$. For the value $P(R,\theta,\varphi)$ the influence of attenuation in the medium can also be taken into account. The corrected coordinates of the point $P(R,\theta,\varphi)$ for consecutive turns in the polar coordinate system, occurring in Eq. (1), can be indicated by the following equations (Opieliński, 2011):

$$\begin{cases} r_i = \sqrt{r^2 + 4R_p^2 \sin^2\dfrac{\beta_i}{2} + 2rR_p\cos(\theta-\beta_i) - 2R_p\cos\theta}, \\ \theta_i = \arctan\left(\dfrac{r\sin(\theta-\beta_i) + R_p\sin(\beta_i)}{r\cos(\theta-\beta_i) + 2R_p\sin^2\frac{\beta_i}{2}}\right), \end{cases} \tag{2}$$

where, due to the necessity to maintain symmetry to the assumed setup of coordinates, $\beta_i = ((n-1)/2 - i)\cdot\beta$ for the variability range $i = 0, ..., n-1$, where $i+1$ denotes the transducer number as shown in Fig. 2. In this paper, it is assumed initially that all transducers are identical and are identically efficient and that their activation takes place at the same time ($t = 0$). Nevertheless, variation of the efficiency of individual transducers of the array is possible by diversifying the proportional acoustic velocity values $V_a(i)$. This model also allows for dynamic focusing and a change in the direction of the ultrasonic wave beam by implementing adequate delays t_i in the factor $e^{j(\omega t_i - kR_i)}$ of formula (1).

4. Results

The ultrasonic ring array was submerged in distilled water with the temperature of 25°C. Using the electronic focusing method by changing the time of activation of the elementary ultrasonic transducers, the radiation axis of focus was changed, which causes the focus to come closer or further apart along the axis between two central transducers and the point where the focus resulting from a natural curvature of the ring array is found. The results of the measurements are shown in Figs 3–5 together with their analyses. On the basis of the acquired images the longitudinal, transverse-angular and contrast resolutions were studied and analysed.

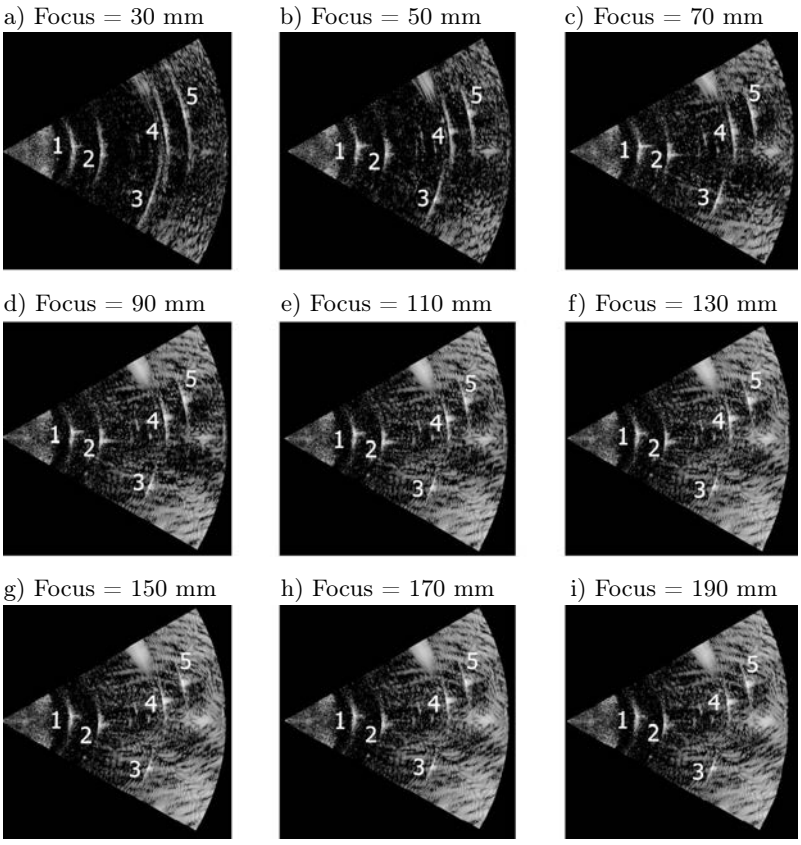

Fig. 3. Measurement results of the wire pattern using the ultrasonic ring array with $n = 32$ activated ultrasonic transducers with the focus at the following intervals: $R = 30$, 50, 70, 90, 110, 130, 150, 170, and 190 mm with numbered echoes coming from the particular wires.

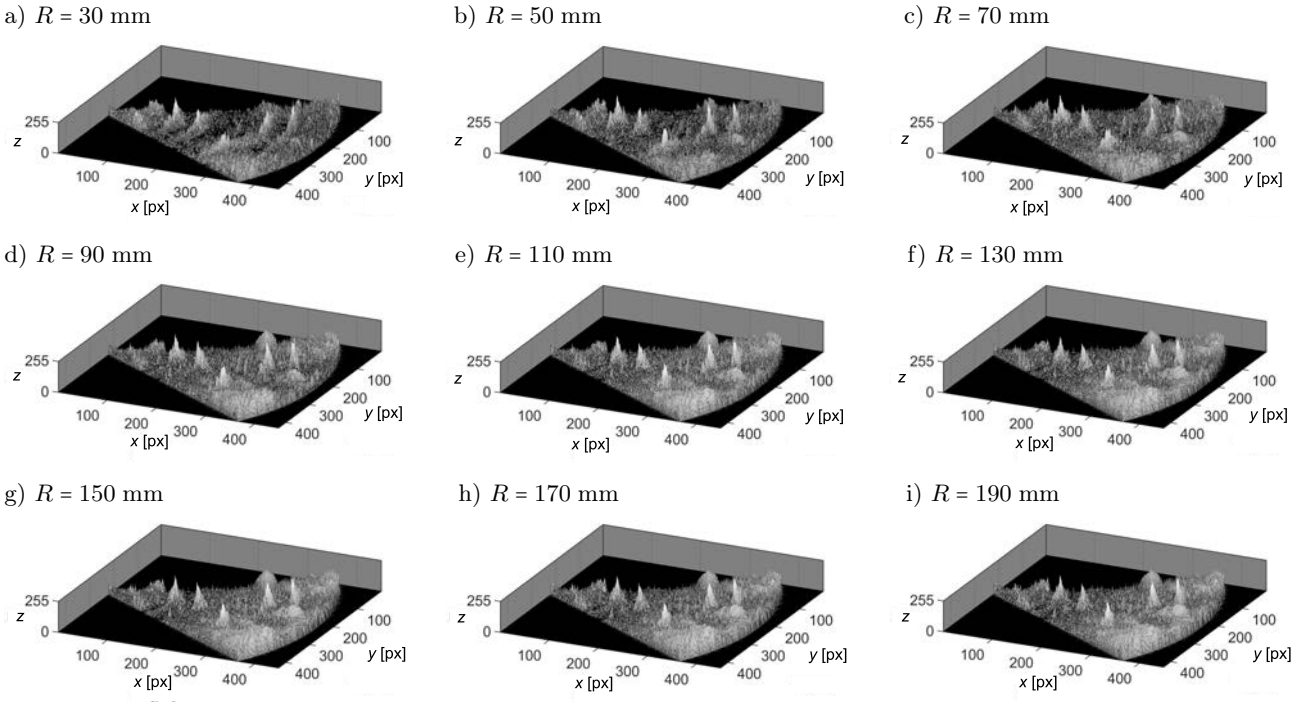

Fig. 4. Three-dimensional visualisation of the measurement results of the wire pattern with electronic focusing settings at the following intervals: R = 30, 50, 70, 90, 110, 130, 150, 170, and 190 mm.

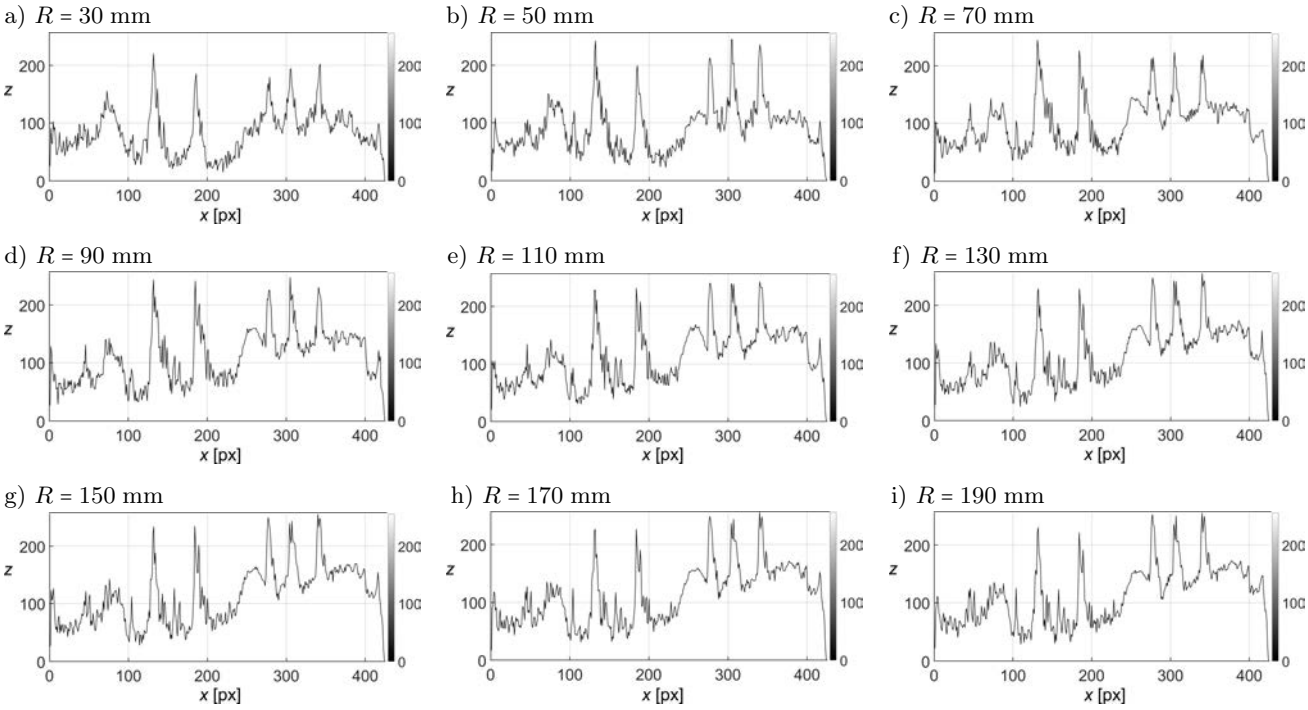

Fig. 5. Graphical representation of echoes coming from the wires of the wire pattern with n = 32 activated ultrasonic transducers with the focus at the following intervals: R = 30, 50, 70, 90, 110, 130, 150, 170, and 190 mm.

The obtained results were compared with acoustic field simulations conducted in the MATLAB software. In order to analyse the acoustic field distribution in individual sections of the ring array (subarray) with varying amounts of activated transducers, the level of acoustic pressure was calculated with the reference pressure value applied in hydroacoustic p_o = 1 μPa. Attenuation in water was not taken into account in the calculations due to its marginal impact on the results. The calculations were made in the range from x = −130 mm to x = 130 mm, and from z = 0 mm to z = 260 mm, setting the ring array in the Cartesian

coordinate system (Staszewski *et al.*, 2018). Since an even number n of transducers in a section is taken into account during calculations, in order to maintain symmetry, the *xyz* coordinate system has been tilted in the horizontal plane to an angle, which allows to set the centre of the system in the axis of symmetry of the transducers. The set range of values x and z enables the visualisation of the acoustic field distribution on the whole interior of the ring array with the radius of R_p = 130 mm. Next, a graphical analysis of the results was conducted. Figure 4 presents a three-dimensional visualisation of acquired two-dimensional images, where the third dimension on the axis is the pixel brightness on the image. Then, a graphical analysis of the pixel brightness was conducted in the scale of 0 to 255 in the form of a cross-section (Fig. 5).

Based on the analysis of Figs 3–5, the conclusion has been drawn that the amplitude of echoes coming from the wires of the wire pattern changes depending on the location of the focus. It has also been noticed that the level of noise increases together with the increase in distance between the focus and central transducers. The lowest levels of noise were recorded for foci R = 30 mm and R = 50 mm (Figs 4ab and 5ab) as well as the greatest brightness of echoes coming from the nearest wires of the wire pattern. Next, an analysis of the acoustic field distribution was conducted using MATLAB software, with the same conditions as with the wire pattern measurements (Figs 6–11).

For the focus closest to central transducers, that is with a distance of 30 mm, the highest level of acoustic pressure in the main lobe of the ultrasonic beam was noted (Fig. 10). On the other hand, the lowest level value of the acoustic pressure was noted for the focus with a distance of 190 mm away from central transducers (Fig. 11). Moreover, together with an increase in the distance between the focus and central transducers the level of acoustic pressure of the main lobe decreases (Figs 10 and 11). It can be noticed that in the case of analysing cross-sections along the main acoustic field distribution beam (for x = 0), the peak level of acoustic pressure for each of the cases falls before the selected focus (Figs 10 and 11) and this shift increases significantly with the focus value increasing. Changes in the location of the focus do not influence the number of lateral lobes nor the width of the main lobe in reference to angular width running along the arc with the radius equal to the distance between the focus and central transducers (Figs 8 and 9).

Analysing the measurements of the wire pattern using the ultrasonic ring array (Fig. 3), the longitudinal and transverse-angular resolutions were studied as well as the brightness of echoes coming from wires of the wire pattern. The wire is presented in the form of an arch on the ultrasonographic image. The coordinates are cylindrical, because the imaging is angular. When marking the length of arch Δl, a fall of 3 dB was taken into account. The analysis was conducted for all re-

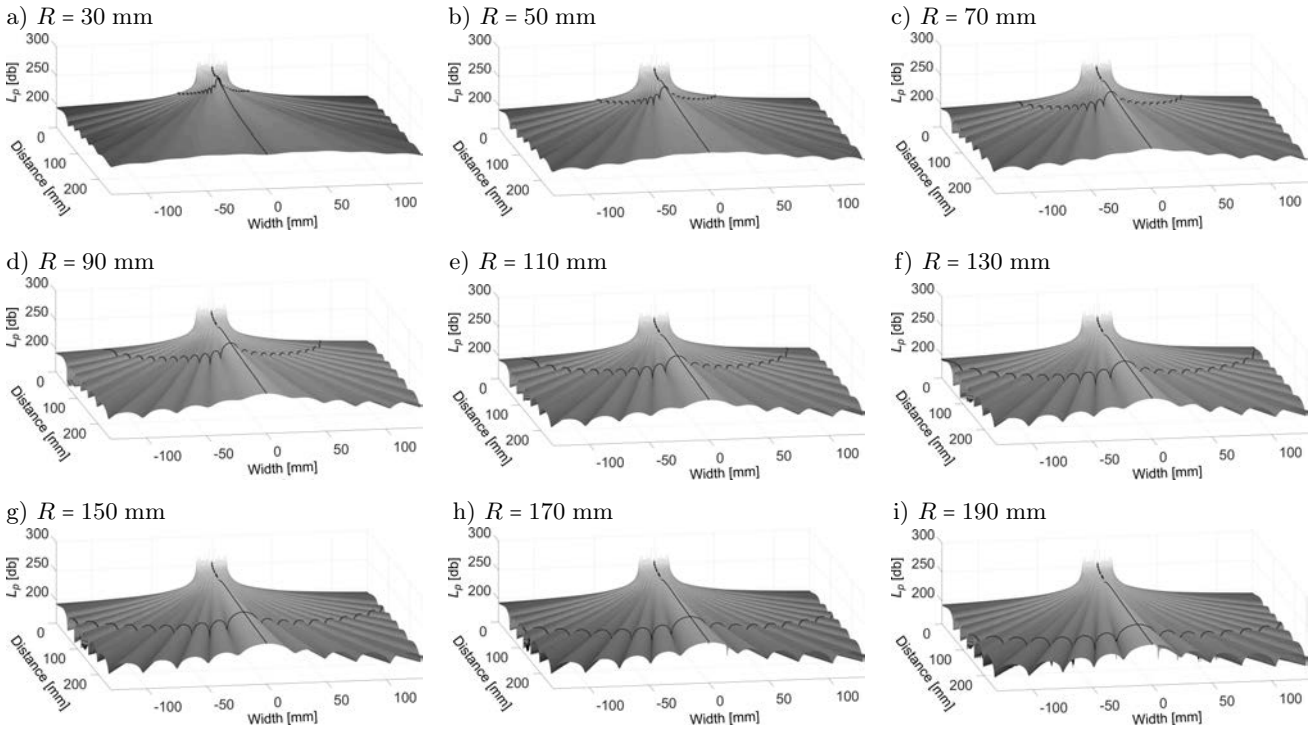

Fig. 6. Results of the acoustic field distribution calculations in the form of $L_p(x, 0, z)$ for sectors of the ring array with n = 32 activated ultrasonic transducers, for foci: R = 30, 50, 70, 90, 110, 130, 150, 170, and 190 mm (in the form of pseudo-three-dimensional graphs).

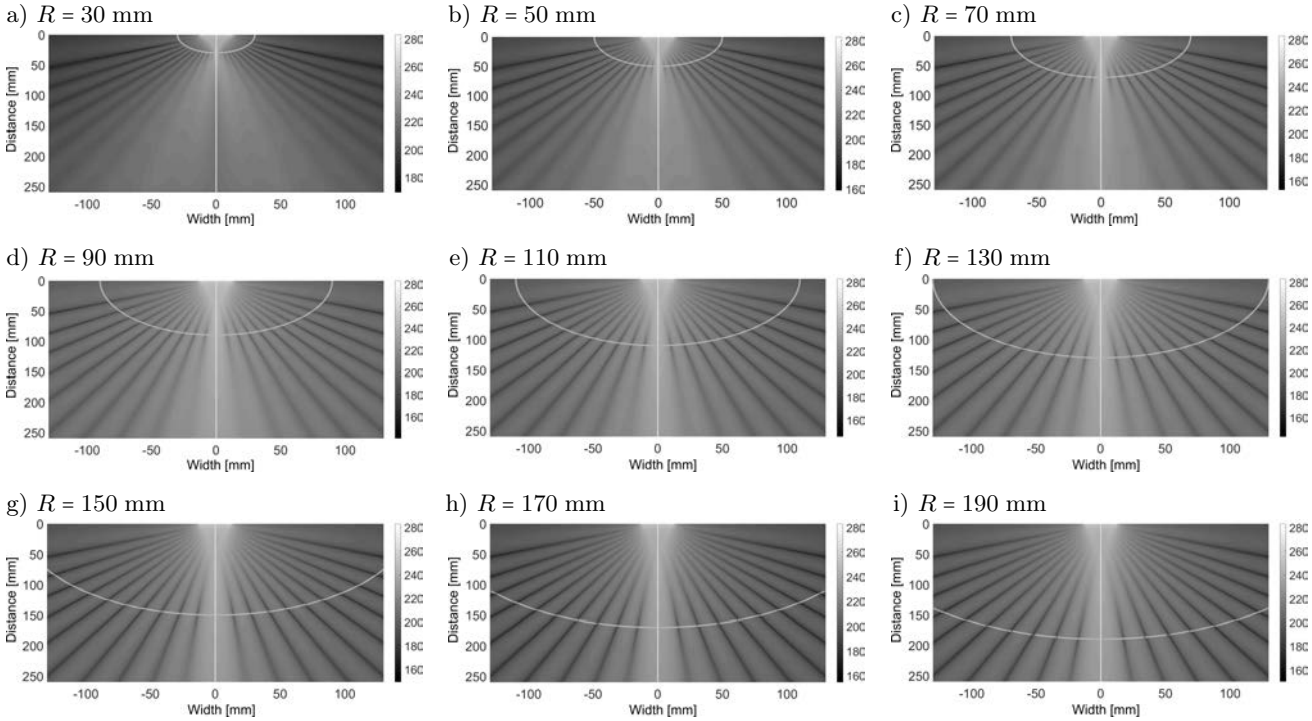

Fig. 7. Results of the acoustic field distribution calculations in the form of $L_p(x, 0, z)$ for sectors of the ring array with $n = 32$ activated ultrasonic transducers for foci: $R = 30$, 50, 70, 90, 110, 130, 150, 170, and 190 mm (in the form of grayscale graphs).

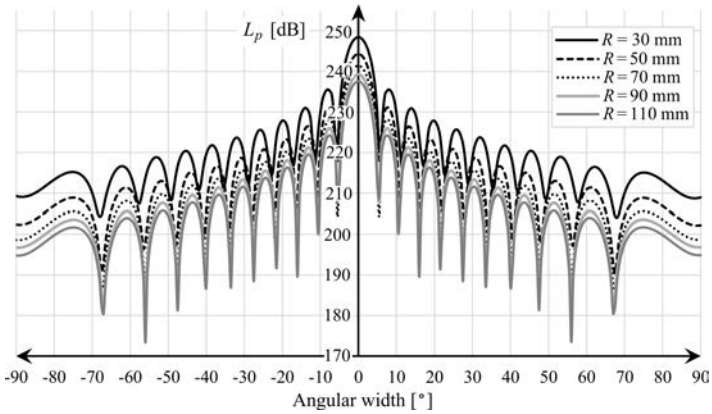

Fig. 8. Results of the acoustic field distribution calculations in the form of $L_p(x)$ with the number of activated transducers $n = 32$, for $y = 0$, $z = R$, for foci $R = 30$, 50, 70, 90, and 110 mm.

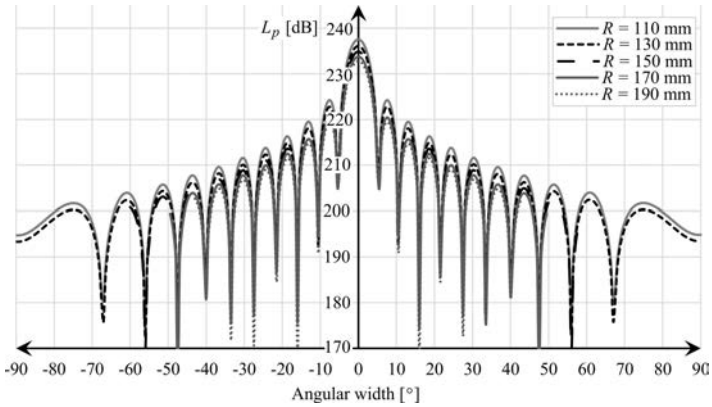

Fig. 9. Results of the acoustic field distribution calculations in the form of $L_p(x)$ with the number of activated transducers $n = 32$, for $y = 0$, $z = R$, for foci $R = 110$, 130, 150, 170, and 190 mm.

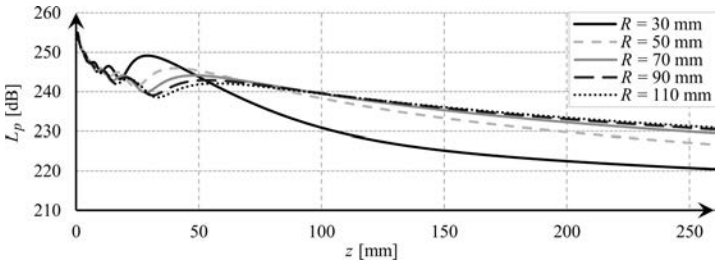

Fig. 10. Results of the acoustic field distribution calculations in the form of $L_p(z)$ with the number of activated transducers $n = 32$, for $x = 0$, $y = 0$, for foci $R = 30$, 50, 70, 90, and 110 mm.

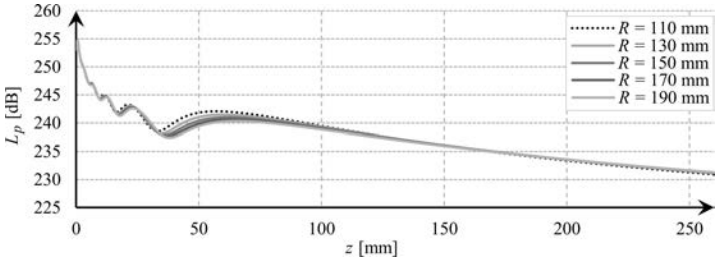

Fig. 11. Results of the acoustic field distribution calculations in the form of $L_p(z)$ with the number of activated transducers $n = 32$, for $x = 0$, $y = 0$, for foci $R = 110$, 130, 150, 170, and 190 mm.

ceived images that varied in the location of the focus resulting from electronic focusing (Fig. 3). The results are shown in Table 1 and in Figs 12–14. The relationship between longitudinal and transverse-angular resolutions are presented for echoes coming from wires of the wire pattern with the numbers 1, 3, and 5.

Table 1. Analysis of the brightness of echoes coming from wires of the wire pattern in a grayscale from 0 to 255 depending on focus location.

Point	1	2	3	4	5
Focus 30	219.9	184.7	178.7	193.8	201.8
Focus 50	241.9	198.8	211.8	244.0	234.9
Focus 70	244.0	225.9	213.8	222.9	217.9
Focus 90	243.0	240.9	224.9	247.0	229.9
Focus 110	227.9	230.9	239.9	238.9	241.9
Focus 130	227.9	227.9	247.0	241.9	254.0
Focus 150	232.9	233.9	249.0	243.0	255.0
Focus 170	225.9	225.9	248.0	243.0	255.0
Focus 190	229.9	220.9	252.0	250.0	255.0

The analysis of ultrasound B-mode images made by the ultrasound tomography ring array demonstrates that the brightest echoes coming from the wires of the measured wire pattern are nearest to the dynamically selected foci. For four of the foci located at a distance of 150, 170, 190, and 200 mm away from central transducers, a maximal level of brightness for echoes coming from wire no. 5 was noted. Whereas, for echoes that came from wires no. 3 and 4 the highest levels of brightness were acquired for the focus 190 mm away from central transducers. By precisely changing the location of the focus inside the ultrasonic ring array, it is possible to identify studied objects or tissues more precisely and to study their parameters.

The analysis of echoes coming from wires of the wire pattern demonstrated that the highest level of brightness for rods no. 1 and 2 was noted during focusing in the range between 50–90 mm away from central transducers, where the level of noise during electronic focusing at a distance of 50 mm away from central transducers (Figs 4b and 5b, Table 1) is much lower in comparison to focusing at a distance of 70–90 mm away from central transducers (Figs 4c, 4d, 5c, 5d, and Table 1). In the case of wires no. 3, 4, and 5, which are located further away from central transducers, electronic focusing further away than the distance of focusing resulting from a natural curvature of the ring array does not significantly influence the quality of echoes coming from the rods, however, the level of noise increases together with an increase in the distance of the focus away from central transducers (Figs 4d–4i, 5d–5i, and Table 1). In the case of focusing at a closer distance of 30–110 mm away from central transducers, the brightness of echoes coming from wires no. 3, 4, and 5 of the wire pattern is lower when compared to the focus at a distance of 130–190 mm (Figs 4a–4i, 5a–5i, and Table 1). The longitudinal resolution for each of the studied wires of the wire pattern and different foci is more or less constant, and the difference between the measurements is maximally 3 mm for any echo registered on the ultrasonographic image. At the same time, the analysis of transverse-angular

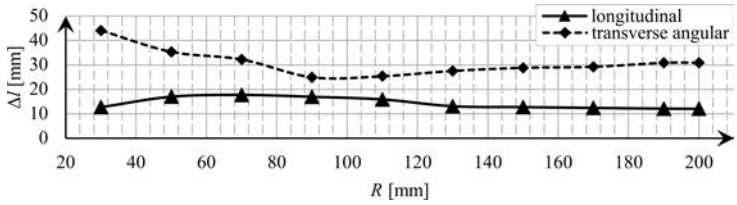

Fig. 12. Results of analysis of longitudinal and transverse-angular resolutions, depending on location of the focus away from central transducers (R [mm]) for echo coming from wire no. 1.

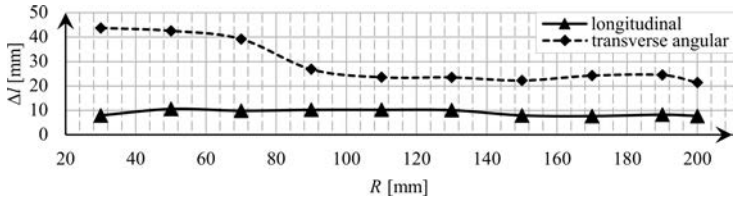

Fig. 13. Results of analysis of longitudinal and transverse-angular resolutions, depending on location of the focus away from central transducers (R [mm]) for echo coming from wire no. 3.

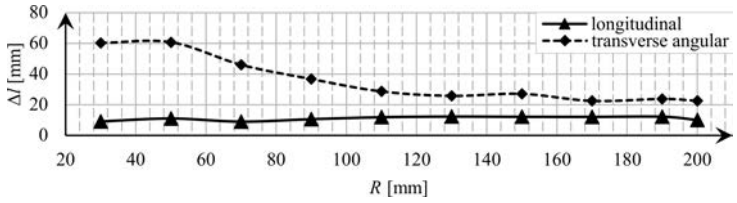

Fig. 14. Results of analysis of longitudinal and transverse-angular resolutions, depending on location of the focus away from central transducers (R [mm]) for echo coming from wire no. 5.

resolution showed that the change of the location of the focus has a significant influence on this value. The closer the location of the focus to central transducers, the worse the transverse-angular resolution will be. Moreover, together with the increase of distance of identified objects (in this case, the wires) away from central transducers, the transverse-angular resolution will increase (improve) regardless of the change in the location of the focus inside the ultrasonic ring array.

In the case when the studied objects do not lie on the axis between the naturally occurring focus and central transducers, it is advisable to study the fields during an inclination of the beam by a set angle. Based on earlier analyses of conducted measurements, it has been concluded before that the brightness of studied objects is higher, the smaller the distance between the focus and the studied point (Table 1). In the next stage of the research a simulation was conducted for the distribution of the acoustic field for a varying number of added transducers and for the inclination of the beam equal to 10°, 20°, and 30°. To do this, it is necessary to calculate the delays in activation in such a way that the wave fronts coming from activated transducers were located at a chosen point at the same time. An analysis was carried out for the beam inclination by 10°, 20°, and 30° in reference to the naturally occurring focus for a varying number of added transducers. Figures 15–20 show the results of these calculations of the acoustic field distribution $L_p(x, 0, z)$ for ring array sectors (subarrays) that are characterised by a varying number of activated transducers (n = 32, 64, 128) in the form of pseudo-three-dimensional graphs.

The analysis of received acoustic field distributions demonstrates that the shape and level of the acoustic pressure of the main and lateral lobes of the ultrasonic beam, after an inclination of the beam, did not undergo a change when compared to earlier results (Staszewski *et al.*, 2018). The inclination of the main lobe by a set angle does not influence its width, whereas the level of acoustic pressure decreases together with an increase in the inclined angle of the beam. Together with the increase in number of added ultrasonic transducers, the peak level of acoustic pressure comes close to the dynamically selected focus. In the case of a small number n = 32 of activated ultrasonic transducers, the peak level of acoustic pressure is found at a distance of 60 mm away from central transducers for natural focusing.

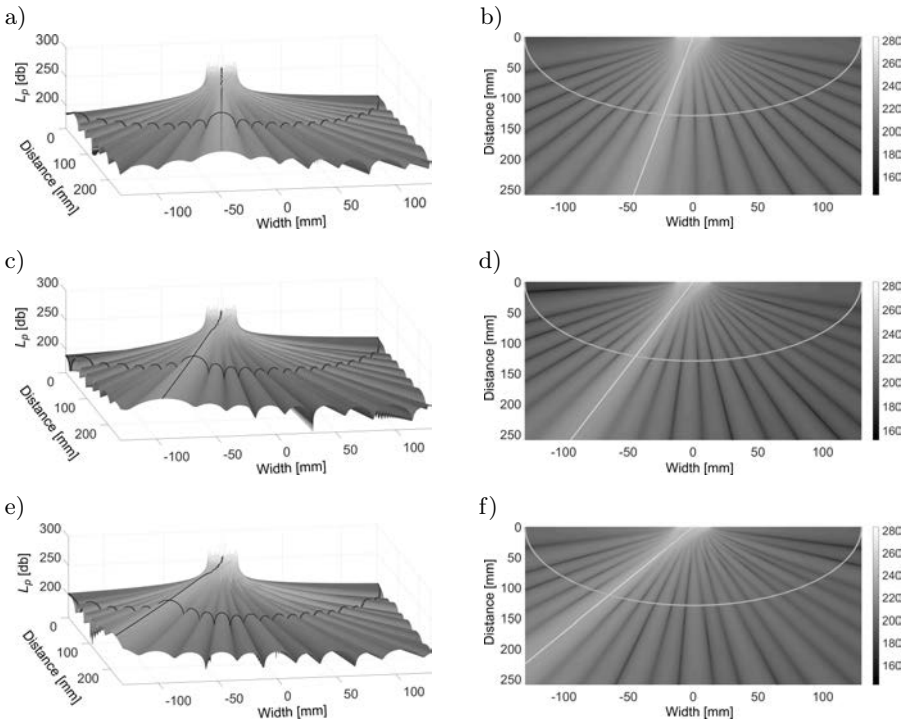

Fig. 15. Results of the acoustic field distribution calculations in the form of $L_p(x, 0, z)$ with the beam inclined by 10°, for the sectors of the ring array with a varying number of n activated transducers and natural focus at the distance of 130 mm: a), b) 32, c), d) 64, e), f) 128.

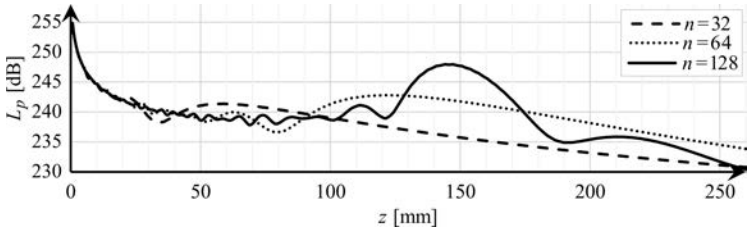

Fig. 16. Results of the acoustic field distribution calculations in the form of $L_p(x)$, $y = 0$, for natural focus $R = 130$ mm inclined by 10°, for the number of activated transducers of the sector as follows: $n = 32$, 64, and 128.

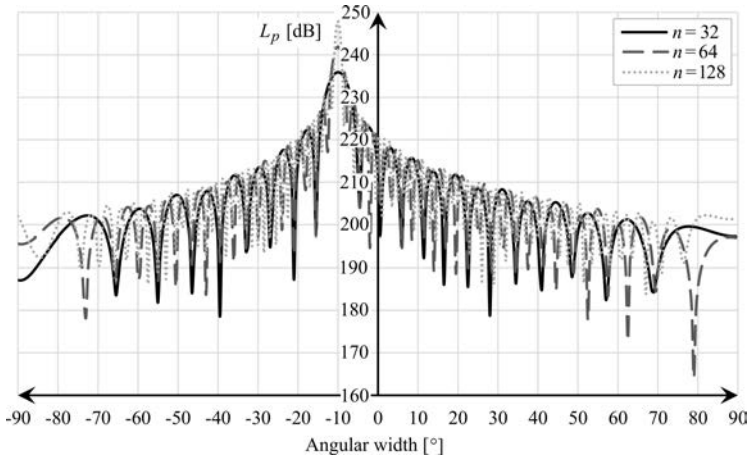

Fig. 17. Results of the acoustic field distribution calculations in the form of $L_p(x)$ for $y = 0$, $z = R = 130$ mm and the focus inclined by 10°, for the number of activated transducers of the sector as follows: $n = 32$, 64, and 128.

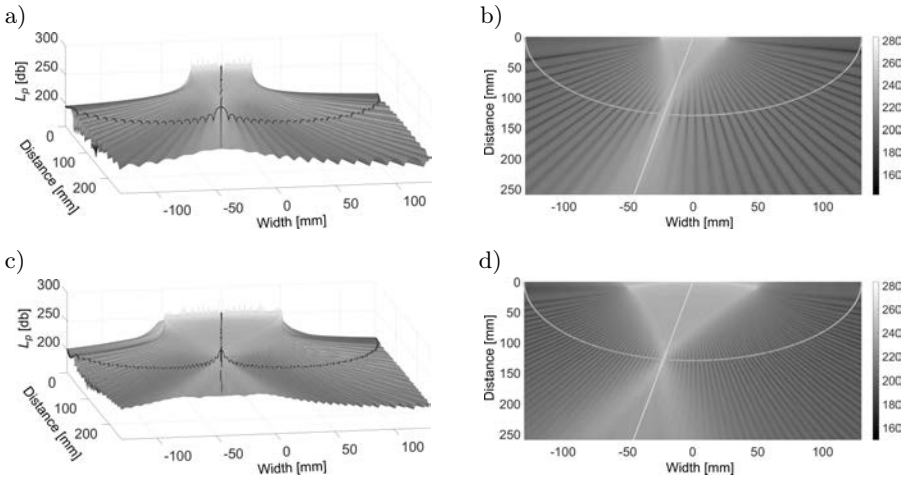

Fig. 18. Results of the acoustic field distribution calculations in the form of $L_p(x, 0, z)$ for sectors of the ring array with the number $n = 32$ of activated transducers and natural focus (130 mm) with the beam inclined by an angle of: a), b) 20°, c), d) 30°.

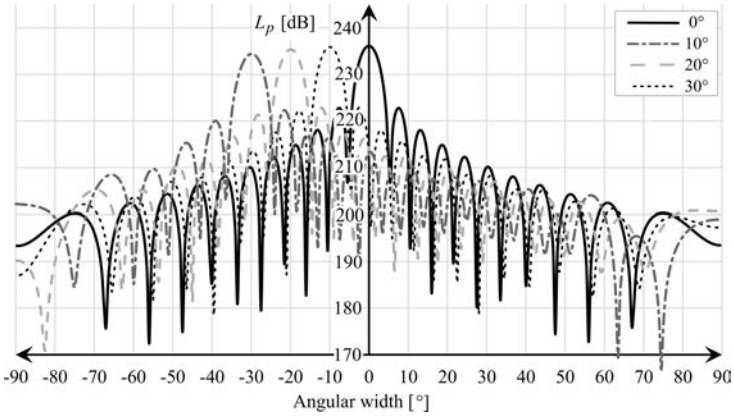

Fig. 19. Results of the acoustic field distribution calculations in the form of $L_p(x)$ for $y = 0$, $z = R = 130$ mm, for $n = 32$ activated transducers in the sector with the beam inclined by an angle of 0°, 10°, 20°, and 30°.

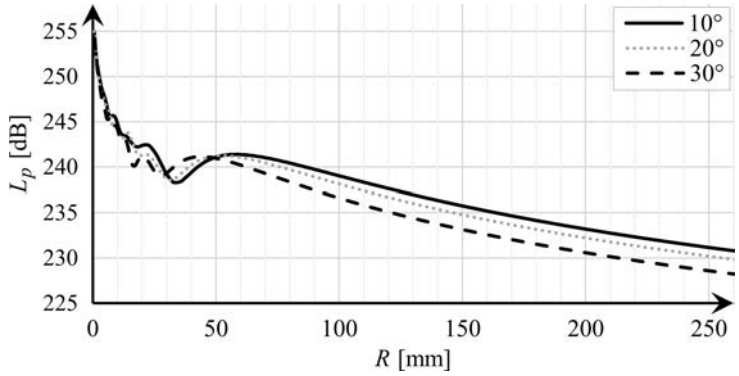

Fig. 20. Results of the acoustic field distribution calculations in the form of $L_p(x)$, $y = 0$, for focus $R = 130$ mm and for $n = 32$ activated transducers in the sector with the angle inclined by 10°, 20°, and 30°.

5. Conclusions

The analysis of measurement results of the wire pattern in the interior of the ultrasonic ring array used in tomography shows that a change in the distance between the focus and central transducers, due to electronic focusing, does not significantly influence the longitudinal resolution of echoes coming from identified wires, whereas the transverse-angular resolution improves together with an increase in the distance be-

tween the focus and central transducers. Moreover, when choosing the optimal setting of the focus, the noise and distortion in ultrasound B-mode images caused by multiple reflections of the ultrasound energy in the transducer ring array should also be taken into account. These reflections are the result of side lobes of the ultrasonic beam. Lateral lobes are located close to the main lobe of the beam due to too big of a distance (pitch) between elementary transducers for used frequency of 2 MHz. These pitches do not meet the condition of half a wavelength, which is required to get the side lobe above the angle of 90°. Therefore, when taking into account the reduction of noise level occurring during focusing as well as the brightness of echoes coming from wires of the wire pattern, it has been concluded that the most optimal focus of the studied foci occurs at a distance of less than 50 mm away from central transducers. In the case of this focus, simulations have also demonstrated a high level of acoustic pressure in a dynamically selected focus in comparison to other studied foci. However, the transverse-angular resolution is getting worse with such a short focus (wires are visible as long arcs) even though the longitudinal resolution is improving. Nevertheless, using the full angle ultrasound spatial compounding of 32 ultrasound B-mode images obtained from 32 angles around the object, distortions in the form of arcs are correlated only in its centres, where the wires actually are. Therefore, the arches will be dimmed in the resulting FASCI image, which results in the improvement of the transverse-angular resolution.

Secondly, in the case of the analysis of the acoustic field distribution for an ultrasonic ring array it has been concluded that the inclination of the main ultrasonic beam in the range of 0° to 30° caused a minor decrease of 2 dB of the acoustic pressure level of the main lobe every 10°, which means that the beam may be inclined by a chosen angle in this range without a deterioration of acoustic field parameters. This enables the application of a wide-angle inclination of the beam for each of the 32 sectors of 32-transducer subarray. Such a wide angle provides a large area of layering of each of the 32 sector images around the breast in the FASCI method, thanks to which a significant reduction of all uncorrelated noise and distortion in images can be achieved by pixel averaging. The level of acoustic pressure in the case of 32 transducers in the range between 130 mm and 260 mm away from central transducers for each of the analysed cases fell by approx. 20 dB. That is why, in the case of focusing at a larger distance exceeding the radius of the ring array, a larger number of transducers should be used.

References

1. Birk M., Kretzek E., Figuli P., Weber M., Becker J., Ruiter N.V. (2016), *High-speed medical imaging in 3D ultrasound computer tomography*. IEEE Transactions on Parallel and Distributed Systems, **27**, 2, 455–467, doi: 10.1109/TPDS.2015.2405508.
2. Duck F.A. (1990), *Physical Properties of Tissue – A Comprehensive Reference Book*, 1st ed. London: Academic Press.
3. Duric N. *et al.* (2007), *Detection of breast cancer with ultrasound tomography: first results with the Computed Ultrasound Risk Evaluation (CURE) prototype*, Medical Physics, **34**, 2, 773–785, doi: 10.1118/1.2432161.
4. Duric N. *et al.* (2013), *Breast imaging with the SoftVue imaging system: first results*, [in:] *Medical Imaging 2013: Ultrasonic Imaging, Tomography, and Therapy*, Proceedings of SPIE, Bosch J.G., Doyley M.M. [Eds], Vol. 8675, p. 86750K-1-8, doi: 10.1117/12.2002513.
5. Entrekin R., Jackson P., Jago J.R., Porter B.A. (1999), *Real time spatial compound imaging in breast ultrasound: technology and early clinical experience*, Medicamundi, **43**, 3, 35–43.
6. Gudra T., Opieliński K. (2006a), *The ultrasonic probe for investigating of internal object structure by ultrasound transmission tomography*, Ultrasonics, **44**, Supplement, e679–e683, doi: 10.1016/j.ultras.2006.05.126.
7. Gudra T., Opieliński K. (2006b), *The multi-element probes for ultrasound transmission tomography*, [in:] *Journal de Physique IV (Proceedings)*, Vol. 137, pp. 79–86, doi: 10.1051/jp4:2006137015.
8. Gudra T., Opieliński K.J. (2006c), *A method of visualizing the internal structure of the center and a device for implementing this method* [in Polish: *Sposób wizualizacji struktury wewnętrznej ośrodka i urządzenie do realizacji tego sposobu*], Patent No 210202, Poland.
9. Jirik R. *et al.*, (2012), *Sound-speed image reconstruction insparse-aperture 3-D ultrasound transmission tomography*, IEEE Transactions on Ultrasonics, Ferroelectrics, and Frequency Control, **59**, 2, 254–264, doi: 10.1109/TUFFC.2012.2185.
10. Marmarelis V.Z., Jeong J., Shin D.C., Do S. (2007), *High-resolution 3-D imaging and tissue differentiation with transmission tomography*, [in:] *Acoustical imaging*, André M.P. *et al.* [Eds], Vol. 28, pp. 195–206, Springer Netherlands, Dordrecht, doi: 10.1007/1-4020-5721-0_21.
11. Opieliński K.J. (2011), *Application of Transmission of Ultrasonic Waves for Characterization and Imaging of Biological Media Structures* [in Polish], Printing House of Wroclaw University of Science and Technology, Wroclaw.
12. Opieliński K.J. *et al.* (2015), *Imaging results of multi-modal ultrasound computerized tomography system designed for breast diagnosis*, Computerized Medical Imaging and Graphics, **46**, 2, 83–94, doi: 10.1016/j.compmedimag.2015.02.004.
13. Opieliński K.J. *et al.* (2018), *Multimodal ultrasound computer-assisted tomography: An approach to the recognition of breast lesion*, Computerized Medical Imaging and Graphics, **65**, 102–114, doi: 10.1016/j.compmedimag.2017.06.009.

14. Opieliński K.J. *et al.* (2016), *Breast ultrasound tomography: preliminary in vivo results*, [in:] Piętka E., Badura P., Kawa J., Wieclawek W. [Eds], *Information technologies in medicine*, Vol. 1, Springer International Publishing, pp. 193–205, doi: 10.1007/978-3-319-39796-2_16.

15. Opielinski K.J., Pruchnicki P., Gudra T., Majewski J. (2014), *Full angle ultrasound spatial compound imaging*. In: Proceedings of 7th Forum Acusticum 2014 Joined with 61st Open Seminar on Acoustics and Polish Acoustical Society – Acoustical Society of Japan Special Session Stream [CD-ROM], Krakow: European Acoustics Association (ISSN 2221-3767).

16. Staszewski W., Gudra T., Opieliński K.J. (2018), *The acoustic field distribution inside the ultrasonic ring array*, Archives of Acoustics, **43**, 3, 455–463, doi: 10.24425/123917.

17. Wiskin J. *et al.* (2013), *Threedimensional nonlinear inverse scattering: quantitative transmission algorithms, refraction corrected reflection, scanner design and clinical results*, Proceedings of Meetings on Acoustics, **19**, 1, 075001, doi: 10.1121/1.4800267.